PNAS RESEARCH ARTICLE | BIOCHEMISTRY OPEN ACCESS

Structural basis for binding of *Drosophila* Smaug to the GPCR Smoothened and to the germline inducer Oskar

Jana Kubíková[a], Gabrielė Ubartaitė[a,1], Jutta Metz[a], and Mandy Jeske[a,2]

Edited by Elizabeth Gavis, Princeton University, Princeton, NJ; received March 27, 2023; accepted June 28, 2023 by Editorial Board Member Susan Strome

Drosophila Smaug and its orthologs comprise a family of mRNA repressor proteins that exhibit various functions during animal development. Smaug proteins contain a characteristic RNA-binding sterile-α motif (SAM) domain and a conserved but uncharacterized N-terminal domain (NTD). Here, we resolved the crystal structure of the NTD of the human SAM domain-containing protein 4A (SAMD4A, a.k.a. Smaug1) to 1.6 Å resolution, which revealed its composition of a homodimerization D subdomain and a subdomain with similarity to a pseudo-HEAT-repeat analogous topology (PHAT) domain. Furthermore, we show that _Drosophila_ Smaug directly interacts with the _Drosophila_ germline inducer Oskar and with the Hedgehog signaling transducer Smoothened through its NTD. We determined the crystal structure of the NTD of Smaug in complex with a Smoothened α-helical peptide to 2.0 Å resolution. The peptide binds within a groove that is formed by both the D and PHAT subdomains. Structural modeling supported by experimental data suggested that an α-helix within the disordered region of Oskar binds to the NTD of Smaug in a mode similar to Smoothened. Together, our data uncover the NTD of Smaug as a peptide-binding domain.

posterior patterning | maternal-to-zygotic transition (MZT) | hedgehog (HH) signaling | nanos mRNA regulation | spmd

Significance

In many animals, early embryonic development relies on maternally deposited gene products. Smaug protein is a key regulator of posterior patterning and crucial for the maternal-to-zygotic transition (MZT) of gene expression of the early *Drosophila* embryo. However, molecular insight into how Smaug binds to its protein interaction partners was lacking. Here, we present the crystal structure of a previously uncharacterized protein domain and provide the structural basis for binding of Smaug to the Hedgehog signaling transducer Smoothened and to the germline inducer Oskar. Molecular insight into these complexes should facilitate future mechanistic studies of Smaug and its partners for a better understanding of their functions during early development.

During oogenesis and early embryogenesis, maternally deposited mRNAs and proteins determine the developmental program in many animals. Over this period of time, the genome is transcriptionally silent, and the expression of genes is regulated at the post-transcriptional level by the modulation of mRNA translation, localization, and stability (1–3). Regulated mRNAs often carry specific *cis*-elements which are recognized by *trans*-acting RNA-binding proteins or microRNAs (miRNAs) that regulate a transcript's fate (4, 5).

Drosophila Smaug and its metazoan orthologs comprise a family of mRNA repressor proteins that contain a characteristic sterile-α motif (SAM) domain, two "Smaug similarity regions" SSR1 and SSR2 within their N-terminal segment, and a pseudo-HEAT-repeat analogous topology (PHAT) domain C-terminally to the SAM domain (Fig. 1*A*). The SAM domain is one of the most abundant protein–protein interaction domains (6–8). In Smaug orthologs, however, it serves as an RNA-binding domain and recognizes mRNA targets by binding to defined stem-loop structures, designated "Smaug recognition elements" (SREs) (9–16). The SSR2 appears limited to metazoan Smaug orthologs, while the SSR1 is present also in various other proteins, including F-box proteins, and was shown to form homodimers (17). The functions of the SSR2 and the PHAT domain remained unclear.

In animals, members of the Smaug protein family exhibit various functions during development. Mammals express two Smaug-related paralogs named SAM-domain-containing protein 4A (SAMD4A, a.k.a. Smaug1) and SAMD4B (a.k.a. Smaug2). A SAMD4A missense mutation in mice causes a lean phenotype, and these animals develop kyphosis associated with myopathy and adipocyte defects and show delayed bone development and decreased osteogenesis (13, 18). Mouse SAMD4B, but not SAMD4A, is present in neuronal precursors of mouse embryos and inhibits neurogenesis in the embryonic cortex (9).

Drosophila Smaug mediates translation inhibition and degradation of bulk *nanos* mRNA in the early *Drosophila* embryo, a critical step during embryonic patterning (19–21). Smaug mediates its effects by recruiting the eIF4E-binding translation inhibitor Cup and the CCR4–NOT deadenylase complex (22–27). Several other RNA-binding proteins have been implicated in Smaug-mediated repression of *nanos* mRNA, including Argonaute 1 (Ago1), Trailer Hitch (Tral), and the DEAD-box RNA helicases "Maternal expression at 31B" (Me31B; ortholog of human DDX6) and Belle (ortholog of human DDX3X/DDX3Y) (22, 28). At the posterior pole of the *Drosophila* embryo, a small fraction of localized *nanos* mRNA escapes Smaug-mediated repression through the activity of Oskar protein (19, 20, 23, 26). The resulting restriction of *nanos* mRNA translation to the

Author affiliations: [a]Biochemistry Center, Heidelberg University, Heidelberg 69120, Germany

Author contributions: M.J. designed research; J.K., G.U., J.M., and M.J. performed research; J.K., G.U., J.M., and M.J. analyzed data; M.J. acquired funding; and M.J. wrote the paper with input from J.K.

The authors declare no competing interest.

This article is a PNAS Direct Submission. E.G. is a guest editor invited by the Editorial Board.

[1]Present address: Structural and Computational Biology Unit, European Molecular Biology Laboratory, Heidelberg 69117, Germany.

[2]To whom correspondence may be addressed. Email: jeske@bzh.uni-heidelberg.de.

This article contains supporting information online at https://www.pnas.org/lookup/suppl/doi:10.1073/pnas.2304385120/-/DCSupplemental.

Published July 31, 2023.

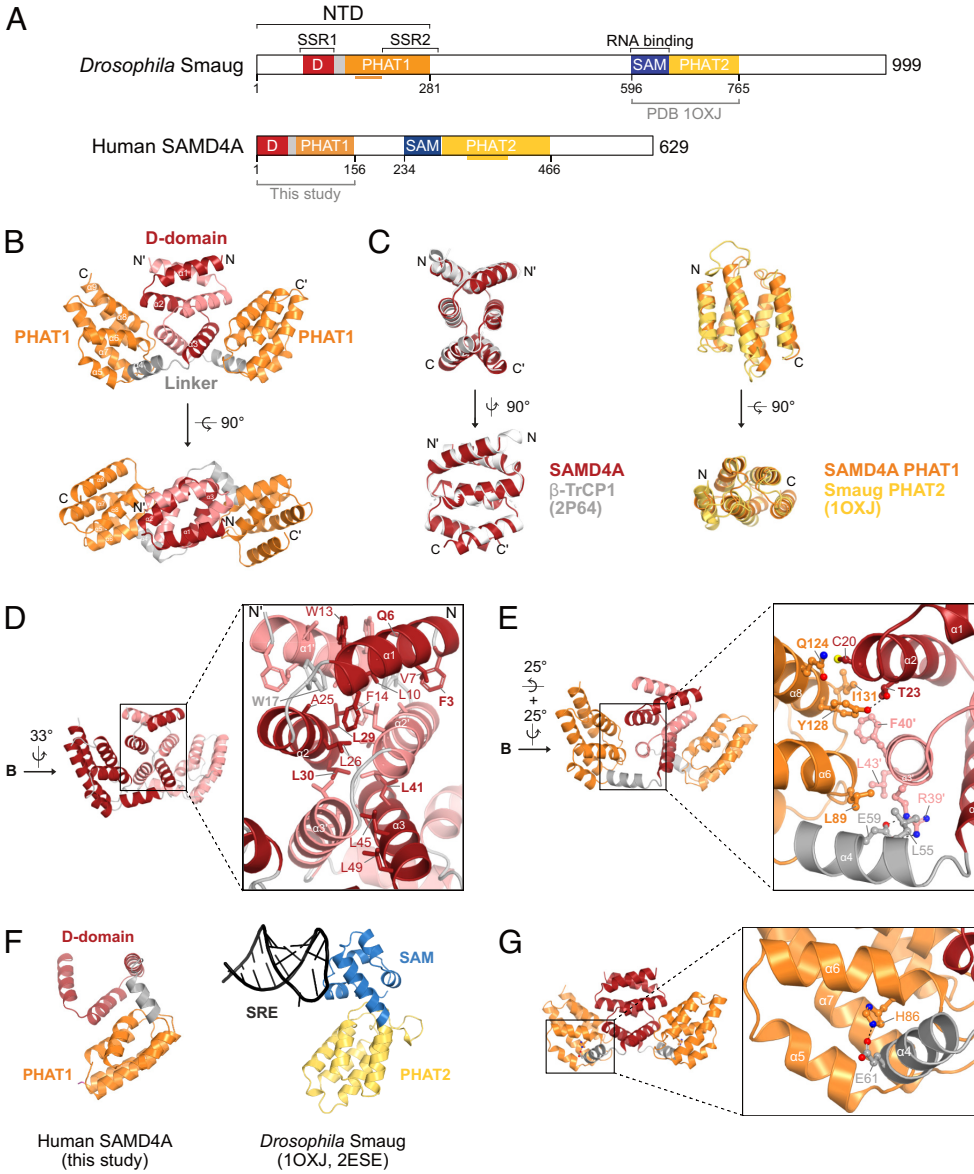

Fig. 1. Crystal structure of the NTD of human SAMD4A. (*A*) Domain organization of *Drosophila* Smaug and human SAMD4A proteins. SSR, Smaug similarity region; NTD, N-terminal domain. The horizontal orange or yellow lines below the protein schemes indicate insertions into the respective PHAT domains. (*B*) Crystal structure of the NTD dimer of the human SAMD4A. The D subdomain, the PHAT1 subdomain, and the linker α-helix are indicated. (*C*) Structural superimposition of the D subdomains of SAMD4A onto the D domain of β-TrCP1 (*Left*) and of the PHAT1 domain of SAMD4A onto the PHAT2 domain of Smaug (*Right*). PDB codes are indicated in parentheses. (*D*) Details of the D subdomain dimer interface of SAMD4A. Amino acid residues are labeled for one protein chain only. Residues in bold are 100% conserved across animals. The orientation of the structure is relative to the one depicted in the *Upper* panel of Fig. 1*B*. (*E*) Details of the interface formed by the D and the PHAT1 subdomains. Residues in bold are 100% conserved across animals. The orientation of the structure is relative to the one depicted in the *Upper* panel of Fig. 1*B*. (*F*) Structural comparison between the D-PHAT1 domain of SAMD4A and the SAM-PHAT2 domain of Smaug. SRE, Smaug recognition elements. The model of the SAM-PHAT2 domain–SRE complex was prepared by superimposition of the two crystal structures indicated by the PDB codes in parenthesis. (*G*) Structural detail indicating the position of the H86 residue, which is mutated in *spmd* mice.

posterior pole gives rise to a Nanos protein gradient that determines the position of abdominal structures in the early embryo (29–32). Several lines of evidence suggest that Oskar might antagonize Smaug-mediated repression by interacting with *nanos* mRNA and/or Smaug (20, 23, 26). Yet, the molecular mechanisms underlying the Oskar-dependent derepression of *nanos* mRNA at the posterior pole of the embryo remain unclear.

In addition to *nanos* mRNA, Smaug acts on many other target transcripts during early embryogenesis and plays a key role in the maternal-to-zygotic transition (MZT) of gene expression, syncytial cell cycle control, blastoderm cellularization, and gastrulation (33–36). Smaug protein is highly abundant during the first 3 h of embryogenesis (20, 37, 38). Later in embryogenesis, with the onset of zygotic transcription, Smaug protein is targeted by a Skp/Cullin/F-box-containing (SCF) ubiquitin E3 ligase complex and is subsequently degraded by the ubiquitin–proteasome system, a process required for an orderly MZT (37, 39).

Through studies in cultured *Drosophila* CI8 cells, in *Drosophila* wing imaginal discs, and in *Drosophila* wings, Smaug has been linked to the Hedgehog (HH) signaling pathway (40). It was shown that Smaug binds to Smoothened, a protein that is structurally similar to Frizzled-type G-protein-coupled receptors (GPCRs) and essential for the transduction of the HH signal (41). The recruitment of Smaug to Smoothened was proposed to result

in phosphorylation of Smaug by the protein kinase Fused (40). Whether the Smaug–Smoothened interaction and the phosphorylation of Smaug play a role during early embryonic development has not been addressed.

Here, we performed a protein–protein interaction screen and confirmed that Oskar and Smoothened directly bind Smaug. Both proteins associated with the previously uncharacterized N-terminal domain (NTD) of Smaug comprising both SSR1 and SSR2. We have solved the crystal structures of the NTD of the human Smaug ortholog SAMD4A alone and of the NTD of *Drosophila* Smaug in complex with a Smoothened peptide. The crystal structures revealed that the NTD is composed of a dimerization (D) subdomain and a PHAT subdomain, which interact and jointly form a groove that is bound by the Smoothened peptide. Furthermore, we identified a predicted α-helix within the disordered region (DR) of Oskar that binds to the NTD of Smaug, and structural modeling supported by experimental data suggests that the complex is structurally similar to the Smaug–Smoothened complex. Together, our data uncover the structural basis for the complex formation between an RNA-binding protein and a signaling protein and suggest a conserved function of the NTD of Smaug proteins as a peptide-binding domain.

Results

Crystal Structure of the NTD of Human SAMD4A. We sought to determine the three-dimensional structure of the uncharacterized NTD (aa 1-281) of *Drosophila* Smaug by X-ray crystallography. Initially, we attempted to crystallize variants of the NTD with N-terminal truncations (Δ1-36, Δ1-69), lacking regions predicted to be disordered (Δ156-196, Δ175-184, Δ159-184), or combinations thereof, but none yielded diffracting crystals. As an alternative, we purified and crystallized the NTD (aa 2-156) of the human Smaug ortholog SAMD4A (Fig. 1*A*) as a hexahistidine (His)-tag fusion. The crystals obtained diffracted to 1.62 Å resolution, and additional diffraction experiments using selenomethionine-derivative crystals allowed us to solve the structure by native phasing methods (*SI Appendix*, Table S1).

The crystal structure revealed that the SAMD4A-NTD forms a homodimer, and each protomer is composed of two subdomains (Fig. 1*B*). The N-terminal subdomain is composed of three α-helices that exhibit a zig-zag arrangement and has previously been predicted to form a dimerization domain similar to the D domain of the β-transducin repeat-containing protein 1 (β-TrCP1) (17). In fact, a search with the protein structure comparison server DALI (42) revealed that the D subdomain of SAMD4A is structurally most similar to the D domain of β-TrCP1. Both D domain dimers aligned with a RMSD of 1.02 Å over 96 aligned Cα-atoms (Fig. 1*C*, *Left*). Within the dimer, the two D subdomains are extensively interlaced to establish a superhelical tertiary structure. The hydrophobic dimer interface is highly conserved (Fig. 1*D* and *SI Appendix*, Fig. S1*A*) and buries a surface area of 2,645 $Å^2$ as determined using the PISA server (43). Attempts to interfere with dimerization through point mutagenesis led to insoluble protein in recombinant expression experiments (*SI Appendix*, Fig. S2).

The C-terminal subdomain of the SAMD4A-NTD is composed of a bundle of five α-helices (α5-9), which is connected with the D subdomain through a linker α-helix (α4) (Fig. 1*B*). DALI search revealed that the five-helical bundle of SAMD4A is structurally most similar to the previously described PHAT domain in the middle part of *Drosophila* Smaug (12) (Fig. 1*A*). Thus, the crystal structure of the SAMD4-NTD led to the finding that both Smaug and SAMD4A contain not one but two PHAT domains: PHAT1 is connected to a D subdomain and located in the NTD, whereas PHAT2 is connected to an RNA-binding SAM domain and located in the middle part of the protein. Sequence alignment and secondary structure prediction analysis revealed that, depending on the protein, PHAT domains are either compact or carry unstructured insertions: The PHAT1 domain of SAMD4A is compact, while the PHAT1 domain of Smaug contains an unstructured insertion; in contrast, the PHAT2 domain of Smaug is compact, while the PHAT2 domain of SAMD4A carries an unstructured insertion (*SI Appendix*, Fig. S3 *A* and *B*). The crystal structures of SAMD4A-PHAT1 and Smaug-PHAT2 aligned with an RMSD of 2.92 Å over 88 Cα-atoms (Fig. 1*C*). The *Saccharomyces cerevisiae* ortholog Vts1 lacks both PHAT domains (*SI Appendix*, Fig. S3*C*).

In the SAMD4A-NTD structure, the PHAT1-domain contacts both protomers of the D subdomain dimer—the one in the same polypeptide chain and its dimerizing partner molecule (Fig. 1*E*). Furthermore, the residues of the interface between the D and PHAT1 subdomains are highly conserved (*SI Appendix*, Fig. S1). We therefore assume that the PHAT1 subdomain might fold back to the D subdomain only after the dimer has been established. A rigid arrangement has also been discussed previously for the relative position of the PHAT2 domain to the SAM domain of Smaug (12) (Fig. 1*F*).

A point mutation in mouse SAMD4A causes a *supermodel (spmd)* phenotype with mice being resistant to obesity induced by a high-fat diet, and displaying leanness and myopathy (18). The *spmd* mutation (H86P) maps to the NTD of SAMD4A, and we analyzed the mutation using our structure of the human SAMD4A-NTD. With the exception of two residues, the sequences of the NTDs (aa 1-155) of human and mouse SAMD4A are identical (*SI Appendix*, Fig. S1*A*). Our structure revealed that His86 resides within the α6-helix of the PHAT1 domain and is engaged in a hydrogen bond with Glu61 residing in the linker α4-helix (Fig. 1*G*). Mutating His86 to proline strongly affected expression of both human and mouse SAMD4A-NTD in *Escherichia coli,* which is in stark contrast to the corresponding wild-type constructs, which are highly soluble (*SI Appendix*, Fig. S4). Proline residues can undergo a *cis-trans* -isomerization reaction and are well known for their impact on protein (mis)folding, for example, by partial mis-isomerization or by their ability to induce kinks in α-helices (44). Therefore, we assume that the *spmd* mutation causes folding problems of the SAMD4A-NTD in vivo, which probably leads to misfunctioning of the protein in mice.

Smaug Directly Binds to Smoothened. To potentially uncover a function for the NTD of Smaug, we reevaluated its interaction partners in a candidate approach. We have recently developed ReLo, a cell culture-based protein–protein interaction assay that is based on a subcellular translocation readout and that detects direct interactions specifically (45). In the ReLo assay, the two proteins to be tested for an interaction are fused to red (mCherry) or green (EGFP) fluorescent proteins, coexpressed in *Drosophila* Schneider 2R+ (S2R+) cells, and their subcellular localization is analyzed by confocal fluorescence microscopy. Importantly, the bait protein carries a membrane anchoring domain, and its interaction with a prey protein is visualized by the subcellular relocalization of the prey protein toward the membrane to which the bait protein is anchored. The ReLo assay is particularly suitable for the characterization of interactions with proteins that are large and poorly accessible for biochemical and biophysical studies, such as Smaug (45).

To assess protein interactions with Smaug, we used an mCherry-Smaug construct that carried an N-terminal fusion to a PH domain (45), which directed the localization of Smaug to the plasma membrane. With the ReLo assay, we have previously evaluated through pairwise testing the interaction between Smaug

and the six core subunits of the CCR4–NOT deadenylase complex, which is responsible for the deadenylation of *nanos* mRNA, and have identified the NOT3 subunit as Smaug-binding protein (27). Here, we tested interactions between Smaug and additional proteins involved in *nanos* mRNA repression, including Ago1 and Ago2 (28), Aubergine and Ago3 (46, 47), Cup (24), as well as Me31B, Tral, and Belle (22, 23). However, we did not observe an interaction between Smaug and any of these factors (*SI Appendix*, Fig. S5*A*). In addition to the pairwise testing, the Smaug–Cup interaction was also tested in the presence of eIF4E and/or the translation control element (TCE) of *nanos* mRNA, which contains two SREs. Again, no interaction between Smaug and Cup was observed (*SI Appendix*, Fig. S5*B*).

Recent findings indicated a direct interaction between Smaug and Smoothened (40). Smoothened is a membrane protein and localizes to distinct cytoplasmic vesicles in S2R+ cells; as such, we were able to confirm the Smoothened–Smaug interaction in the ReLo assay by asking whether Smoothened localizes Smaug to these vesicles (Fig. 2 *A* and *B*). We next set out to map the regions of Smaug and Smoothened that are involved in the interaction. Smoothened consists of an N-terminal extracellular cysteine-rich domain (CRD; aa 51-246), a central seven-transmembrane domain (7-TM; aa 247-555), and a C-terminal "cytotail" (aa 556-1036), which is a long cytoplasmic and predominantly DR (Fig. 2*A*). As the cytotail has been previously reported to bind Smaug (40), this fragment of Smoothened was tested in combination with the N-terminal part of Smaug (NTD; aa 1-281), the DR1 (aa 282-595), the SAM-PHAT domain combination (aa 596-765), or the C-terminal DR2 (aa 766-999). The ReLo assay revealed that the Smoothened cytotail bound to the NTD of Smaug (Fig. 2*C*), which is consistent with previous data (40). Using ReLo, we further confirmed previous data that Smaug bound to a small region within the cytotail of Smoothened spanning amino acid residues 958 to 1,003 (40) and refined the mapping to a predicted α-helix covering residues 970-1003 of Smoothened (Fig. 2*D*). By isothermal titration calorimetry (ITC), the K_D of the complex formed by a Smaug-NTD lacking the N-terminal DR (aa 70-281) and a synthetic Smo 970-1003 peptide was determined as 0.8 μM, and the complex was found to have a 1:1 stoichiometry (Fig. 2*E*). In following experiments, we refer to Smoothened 970-1003 as the Smaug-binding region (SBR).

Structure of the NTD of Smaug in Complex with the SBR of Smoothened. Next, we aimed to obtain structural information on the Smaug–Smoothened complex. The cytotail of Smoothened is conserved in Drosophilids but not across animals (*SI Appendix*, Fig. S6*A*), and we have not detected any binding of human or *Drosophila* Smoothened to human SAMD4A (*SI Appendix*, Fig. S6 *B–D*), which suggests that the Smoothened-Smaug interaction is specific to *Drosophila*. To crystallize the *Drosophila* Smaug-NTD in complex with the Smoothened SBR peptide, we designed a Smaug-NTD construct based on the SAMD4A-NTD structure, in which two regions of predicted disorder (Δ1-72 and Δ156-196) were deleted. The *Drosophila* Smaug-NTD harboring these two deletions was able to bind to Smoothened (and Oskar, see below) (*SI Appendix*, Fig. S7). Two strategies were pursued for crystallization: one in which Smaug 70-281Δ156-196 (His-tag removed) was mixed with a Smo 970-1003 peptide and a second in which the Smo 970-1003 sequence was fused to the N terminus of Smaug 73-278Δ156-196 using a $(GGS)_4$ linker. With both strategies, crystals of similar shape were obtained. Of these, the crystals of the single-chain construct diffracted best and to 2.0 Å resolution (*SI Appendix*, Table S1). The structure of the Smaug–Smoothened complex was solved by molecular replacement using the human SAMD4A-NTD structure as a search model. The resolved structure was composed of two molecules each of Smaug 73-274Δ156-196 and Smo 976-989; no electron density was observed for the $(GGS)_4$ linker (Fig. 3*A*).

The Smoothened peptide forms an α-helix, which is bound to a groove created by the D subdomain dimer and the PHAT subdomain. The interface area of the Smaug–Smoothened complex measures 1,522 $Å^2$ (43) (Fig. 3*B*). The Smoothened α-helix that binds to Smaug is highly conserved across Drosophilids but not in higher animals (Fig. 3*C* and *SI Appendix*, Fig. S6*A*). The Smaug–Smoothened interface was validated by mutational analyses: The triple point mutation L978E/L984E/L985E in Smoothened interfered with Smaug binding

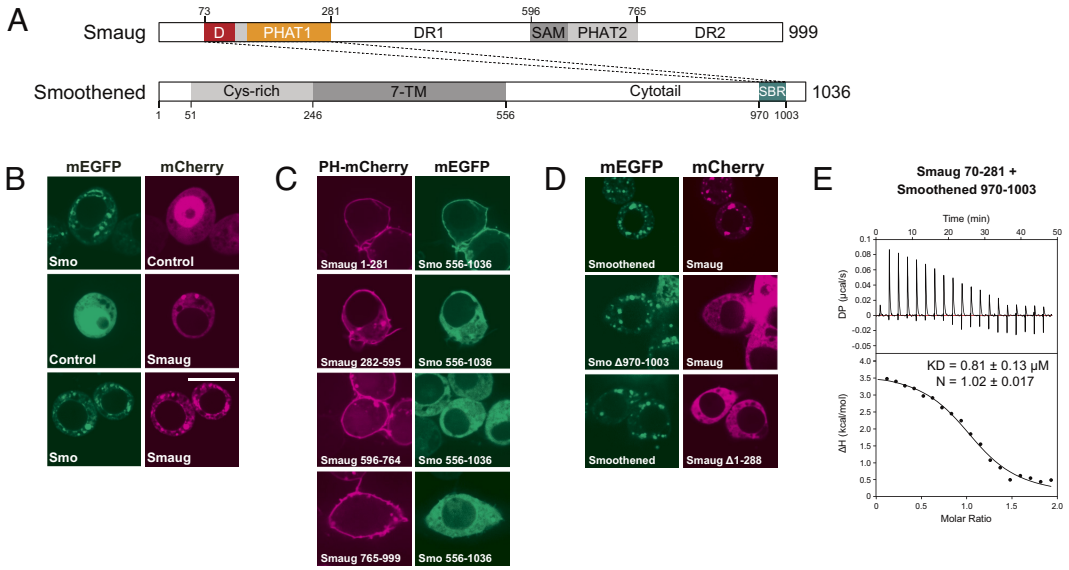

Fig. 2. The Smaug–Smoothened interaction. (*A*) Domain organization of *Drosophila* Smaug and Smoothened proteins. DR, disordered region; TM, transmembrane; SBR, Smaug-binding region. (*B*) ReLo assays showed a colocalization between Smaug and Smoothened. Controls are plasmids without an insert. (The scale bar is 10 μm.) (*C*) Of the four Smaug fragments indicated, only the NTD (Smaug 1-281) interacted with the Smoothened cytotail (Smo 556-1036) in the ReLo assay. (The scale bar is 10 μm.) (*D*) The Smoothened deletion and the Smaug deletion were unable to interact with Smaug and Smoothened, respectively, in the ReLo assay. (The scale bar is 10 μm.) (*E*) ITC using Smaug NTD (aa 70-281, His-tag removed) and a Smoothened peptide (Smo 970-1003).

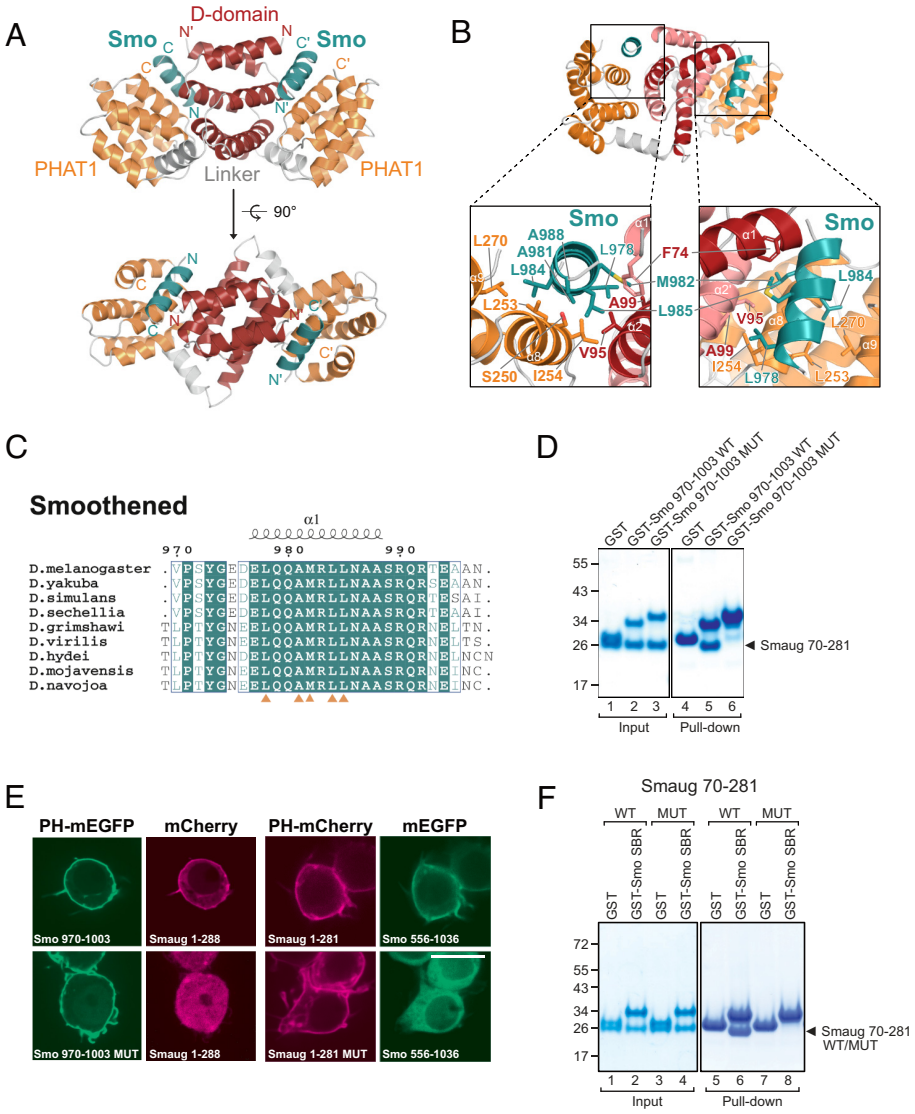

Fig. 3. Crystal structure of Smaug-NTD in complex with Smoothened. (*A*) Crystal structure of the NTD of *Drosophila* Smaug in complex with a Smoothened peptide (colored deep teal). (*B*) Structural detail of the Smaug–Smoothened interface. (*C*) Sequence alignment of the Smaug-binding region of Smoothened. Orange triangles indicate central residues involved in the Smaug interaction. (*D*) GST pull-down assay using 1 nmol GST-Smoothened 970-1003 (SBR) wild-type (WT) or L978E/L984E/L985E mutant (MUT) proteins and 2 nmol Smaug 70-281 (His-tag removed). Protein markers in kDa are indicated on the left. Input and pull-down samples originated from one experiment; the gel was split as it contained also the data shown in *SI Appendix*, Fig. S6*D*. (*E*) Mutant Smoothened SBR (MUT; L978E/L984E/L985E) did not interact with the NTD of Smaug, and mutant Smaug NTD (MUT; S250E/L253E) did not interact with the Smoothened cytotail in the ReLo assay. (The scale bar is 10 μm.) (*F*) GST pull-down assay using 1 nmol GST or GST-Smoothened SBR (970-1003) and 1 nmol Smaug NTD (70-281) wild-type or S250E/L253E mutant proteins (His-tag removed). Protein markers in kDa are indicated on the left. Input and pull-down samples originated from one experiment but were loaded onto two gels.

in ReLo and GST pull-down assays (Fig. 3 *D* and *E*). Likewise, the S250E/L253E mutation in Smaug prevented the interaction with Smoothened in ReLo and GST pull-down assays (Fig. 3 *E* and *F*). Thus, our mutational analysis confirms the interface of the Smaug–Smoothened complex observed in the crystal structure.

Oskar Directly Binds to Smaug. Using ReLo, we also retested the previously described interaction between Smaug and Oskar (20, 23, 26) (for protein schemes see Fig. 4*A*). Translation of *oskar* mRNA from two alternative start codons results in two protein isoforms, of which Short Oskar is essential for germ cell formation and posterior patterning (48). We tested Smaug interaction to the two Oskar isoforms. Long Oskar is a membrane protein (49) and localized as speckles in S2R+ cells (Fig. 4*B*). Thus, we did not use an additional membrane anchor to test the Smaug–Long Oskar interaction in the ReLo assay. When Long Oskar and Smaug were coexpressed, we did not observe a relocalization of Smaug (Fig. 4*B*). Short Oskar localizes to the nucleus in S2R+ cells, and a fusion to the PH domain does not efficiently redirect/anchor Short Oskar to the plasma membrane (45). Therefore, to assess protein interactions to Short Oskar, it carried an N-terminal fusion to OST4, a small membrane protein that directed Short Oskar localization to the endoplasmic reticulum (ER). Using OST4-anchored Short Oskar, we have previously confirmed the known direct interaction with the DEAD-box RNA helicase Vasa (*SI Appendix*, Fig. S8*A*) (45, 50, 51). Here, we show that OST4-Short Oskar interacted also with Smaug (Fig. 4*B*), which is consistent with earlier observations (20, 23, 26). We used additional ReLo assays to test other previously suggested binding partners of Short Oskar, including the WD40 protein Valois (a.k.a. MEP50) (52), the eIF4E-binding protein Cup (53), the actin-binding protein Lasp (54), and the dsRNA-binding protein

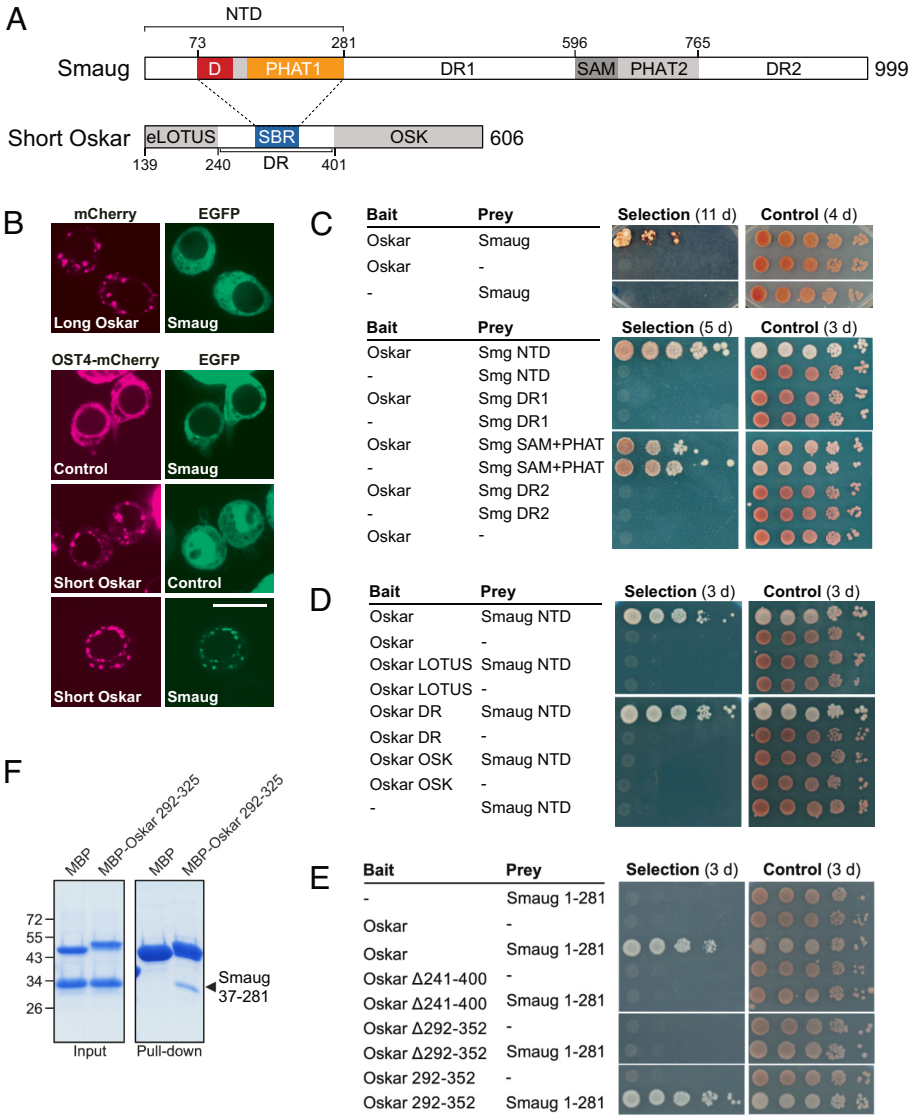

Fig. 4. The Smaug–Short Oskar interaction. (*A*) Domain organization of *Drosophila* Smaug and Oskar. The Short Oskar isoform is generated by alternate translation from M139 onward. NTD, N-terminal domain; DR, disordered region; SBR, Smaug-binding region. (*B*) Smaug interacted with Short Oskar but not Long Oskar in the ReLo assay. Plasmids lacking an insert served as controls. (The scale bar is 10 μm.) (*C*) Oskar (only the short isoform was tested) and Smaug interacted in split-ubiquitin yeast two-hybrid (Y2H) assays (*Upper*). Short Oskar binding mapped to the NTD of Smaug (*Lower*). Ten-fold dilutions are shown. Selection plates lacked adenine and histidine as compared to control plates. (*D*) The NTD of Smaug bound to the DR of Short Oskar in Y2H assays. Ten-fold dilutions are shown. Selection plates lacked adenine and histidine as compared to control plates. (*E*) Oskar 292-352 (SBR) was necessary and sufficient for Smaug-NTD binding in Y2H assays. Ten-fold dilutions are shown. Selection plates lacked adenine and histidine as compared to control plates. (*F*) MBP pull-down assay using 1 nmol His-MBP-Oskar 292-325 and 5 nmol Smaug NTD (37 to 281; His-tag removed). Input and pull-down samples originated from one experiment; the gel was split into two panels as it contained additional data irrelevant to the study.

Staufen (55). However, none of these proteins relocalized with Short Oskar (*SI Appendix*, Fig. S8*B*).

The interaction between Smaug and Short Oskar was also visible in split-ubiquitin yeast-two hybrid (Y2H) assays (Fig. 4 *C*, *Upper*), which we then used to map the respective protein regions that mediate the interaction. Interestingly, among the four Smaug fragments tested, it was the NTD that bound to Short Oskar (Fig. 4*A* and *Lower* panel of Fig. 4*C*), which is the same Smaug domain that also bound to Smoothened. Next, we examined which part of Short Oskar binds to Smaug. Short Oskar carries an extended LOTUS (eLOTUS) domain (aa 139-240) at the N terminus, followed by a predominantly DR (aa 241-400), and a C-terminal OSK domain (aa 401-606) (Fig. 4*A*). Both the eLOTUS and the OSK domain bind to RNA in vitro (51, 56, 57). In addition, the eLOTUS domain serves as a regulatory domain for the Vasa ATPase activity (50). In Y2H experiments, Smaug bound to the DR fragment of Oskar (Fig. 4*D*). Short Oskar that carried a deletion of the DR was not able to interact with the NTD of Smaug (Fig. 4*E*). The DR of Oskar carries several regions with high sequence conservation across Drosophilids (*SI Appendix*, Fig. S8*C*). Of these, Oskar 292-352 was the SBR, as it was necessary and sufficient for Smaug interaction in Y2H assays (Fig. 4*E*). Moreover, a shorter version of the Oskar SBR (aa 292-325), which showed highest conservation (*SI Appendix*, Fig. S8*C*), fused to maltose-binding protein (MBP) was able to pull down the NTD of Smaug (aa 37-281) in an MBP pull-down assay (Fig. 4*F*). Like Smoothened, Oskar bound to the NTD of Smaug, but not to the NTD of SAMD4A (*SI Appendix*, Fig. S8*D*).

Predicted Structure of the SBR of Oskar Bound to the NTD of Smaug. Surface residues of the Smoothened-binding groove of the NTD of Smaug are relatively conserved across animals

(*SI Appendix*, Fig. S1), and we asked whether the SBR of Short Oskar might bind to this groove too. We ran an AlphaFold2-multimer structural prediction (58–60) using two copies each of Smaug 70-280 (NTD) and Oskar 295-330 as input sequences. We obtained a model of a heterotetramer, in which two α-helices covering a part of the SBR of Oskar (aa 292-309) were placed into the Smoothened-binding groove of each D-PHAT domain of Smaug (Fig. 5 *A* and *B* and *SI Appendix*, Fig. S9*A*). This shorter part of the SBR contains several conserved and highly conserved residues that contact the NTD of Smaug (Fig. 5*C*). Importantly, using ReLo and Y2H assays, we found that the interaction between Short Oskar and Smaug is prevented when Oskar lacked the longer or shorter version of the SBR or when Smaug carried the point mutations in the NTD that also disrupted its interaction with Smoothened (Fig. 5 *D*–*F*). Finally, a Smoothened SBR synthetic peptide was able to compete with MBP-Oskar binding to the Smaug-NTD in a GST pull-down assay, while a mutant peptide sequence was not (Fig. 5*G*). Together, these data demonstrated that Smaug binds to Smoothened or Short Oskar in a similar fashion and revealed the NTD of Smaug as a peptide-binding domain.

Discussion

Here, we present the crystal structures of the previously uncharacterized NTDs of human SAMD4A and *Drosophila* Smaug, which are composed of a D and a PHAT subdomain. These structural data revealed that Smaug and its animal orthologs contain not one but two PHAT domains, one connected to the dimerizing D domain and one connected to the RNA-binding SAM domain. The D domain has been predicted previously for Smaug and Vts1, and dimerization of the Vts1 D domain was demonstrated (17). Furthermore, our structural analysis of the Smaug–Smoothened complex revealed that the D domain not only functions as a dimerization domain but also forms a peptide-binding groove together with the PHAT subdomain. As a comparison, we used AlphaFold2 to predict the structural models of the SAMD4A-NTD and of the Smaug-NTD in complex with the Smoothened SBR, which superimposed well with an RMSD of 0.77 Å and 1.02 Å, respectively, with the experimental structures (*SI Appendix*, Fig. S9 *B* and *C*). We further demonstrated an interaction between the Smaug-NTD and a short part of the predominantly DR of Oskar. Structural prediction revealed a binding mode for the Oskar–Smaug interaction that is similar to the Smoothened–Smaug complex (*SI Appendix*, Fig. S9*A*). The formation of such a protein binding groove is probably specific to the animal members of the Smaug protein family, as yeast Vts1 contains the D and the SAM domains but lacks PHAT domains. The high conservation of the protein-binding groove of the NTD of metazoan Smaug/SAMD4 proteins suggests that SAMD4A, which does not bind to Oskar or Smoothened, may bind to a yet unknown partner in a similar fashion (Fig. 5*H*).

Previously, a direct Oskar–Smaug interaction has been suggested and mapped to the SAM-PHAT2 domain of Smaug using classical Y2H assays (20). The data from this interaction mapping raised the idea that Oskar might antagonize the Smaug repressive function by competing with the *nanos* SREs for binding to the RNA-binding SAM domain of Smaug (20). However, the same lab also created transgenic flies to test mutations in Smaug that might interfere with Oskar interaction, without affecting RNA binding, and reported that these substitutions had no effect on embryonic patterning (62). Using the split-ubiquitin-based Y2H, we did not observe a specific interaction between the SAM-PHAT2 region of Smaug and Short Oskar: We observed a similar degree of cell growth when the SAM-PHAT construct was coexpressed with the control plasmid as compared to its coexpression with Short Oskar. Instead, we found that Oskar bound to the NTD of Smaug. Dahanukar et al. (20) did not test a Smaug fragment comprising the full NTD, but only a truncated fragment (aa 1 to 242) lacking a large part of the PHAT1 subdomain. This truncated Smaug construct did not show an Oskar interaction (20). Our Y2H data, structural modeling, and mutagenesis all lead to the conclusion that Oskar binds to the NTD of Smaug, but it remains unclear whether this interaction contributes to a block of Smaug binding to *nanos* mRNA, and if so, how. As Oskar did not bind to the RNA-binding SAM domain of Smaug, and the NTD of Smaug did not bind to RNA in in vitro binding experiments (*SI Appendix*, Fig. S10), Oskar seems not to actively interfere with binding of Smaug to *nanos* mRNA. UV cross-link experiments indicate that Short Oskar binds to *nanos* mRNA in vivo (51). However, from this experiment, it is unclear whether Oskar is capable of recognizing *nanos* mRNA directly or whether the RNA-binding specificity is mediated by another RNA-binding protein in vivo, such as Smaug. The eLOTUS domain of Short Oskar binds to the DEAD-box RNA helicase Vasa and stimulates its ATPase activity (50), suggesting a contributing function of Vasa in *nanos* mRNA control. Whether indeed Oskar works together with Vasa to prevent the Smaug-mediated repression of *nanos* mRNA at the posterior pole remains to be investigated.

Our biochemical and structural data demonstrate a direct interaction between Smoothened and Smaug, yet the function of this interaction is unclear. In cell culture assays, Smaug is phosphorylated upon HH signaling, and this phosphorylation depends on Smoothened (40). Further studies in cell culture, in wing imaginal discs, and fly wings suggested that Smaug phosphorylation leads to a reduced mRNA repressive activity (40). Smaug has an established function as a repressor of maternal mRNAs during early *Drosophila* embryogenesis. Consistent with this function, Smaug protein expression is highest between 0 and 3 h of embryonic development (20, 63, 64) (*SI Appendix*, Fig. S11*A*). In contrast, Smaug protein levels are at the detection limit in all developmental stages beyond the larvae stage L3 (64) (*SI Appendix*, Fig. S11*A*), and Smaug defects were reported earlier to not cause any phenotype in the adult fly (20).

Keeping these earlier observations in mind, we asked whether there might be a function for the Smaug–Smoothened interaction in the early embryo. During early embryogenesis, the protein expression pattern of Smoothened is reciprocal to the one of Smaug: Smoothened protein levels are low in early embryos and strongly enhanced after 3 h of development (64, 65) (*SI Appendix*, Fig. S11*A*). This reciprocal expression pattern might indicate that one protein regulates the level of the other protein. Smaug protein is actively cleared during the MZT (after ca. 3 h), and its degradation is initiated by SCF-mediated ubiquitination (37, 39). Furthermore, it was suggested that Smaug is recognized by the F-box proteins Slmb (the *Drosophila* β-TrCP ortholog) and Bard, with Bard exhibiting a predominant and a timing role in Smaug degradation (37, 39). In our ReLo assays, we did not observe the Smaug–Slmb interaction but detected the Smaug–Bard interaction (*SI Appendix*, Fig. S11*B*). Often the recognition of target proteins by F-box proteins, such as Slmb, depends on prior phosphorylation of the target (66–69). Mouse and human SAMD4A/Smaug1 were reported to interact with 14-3-3 proteins (18, 70), a protein family known to recognize phosphorylated sequences within their protein partners (71). We detected the *Drosophila* Smaug interaction to 14-3-3ζ and 14-3-3ε in our ReLo assays (*SI Appendix*, Fig. S11*C*), suggesting that Smaug is phosphorylated in these cells. Furthermore, Smaug phosphorylation has been described in the embryo and in *Drosophila* Cl8 cell culture (40, 72). In Cl8 cells,

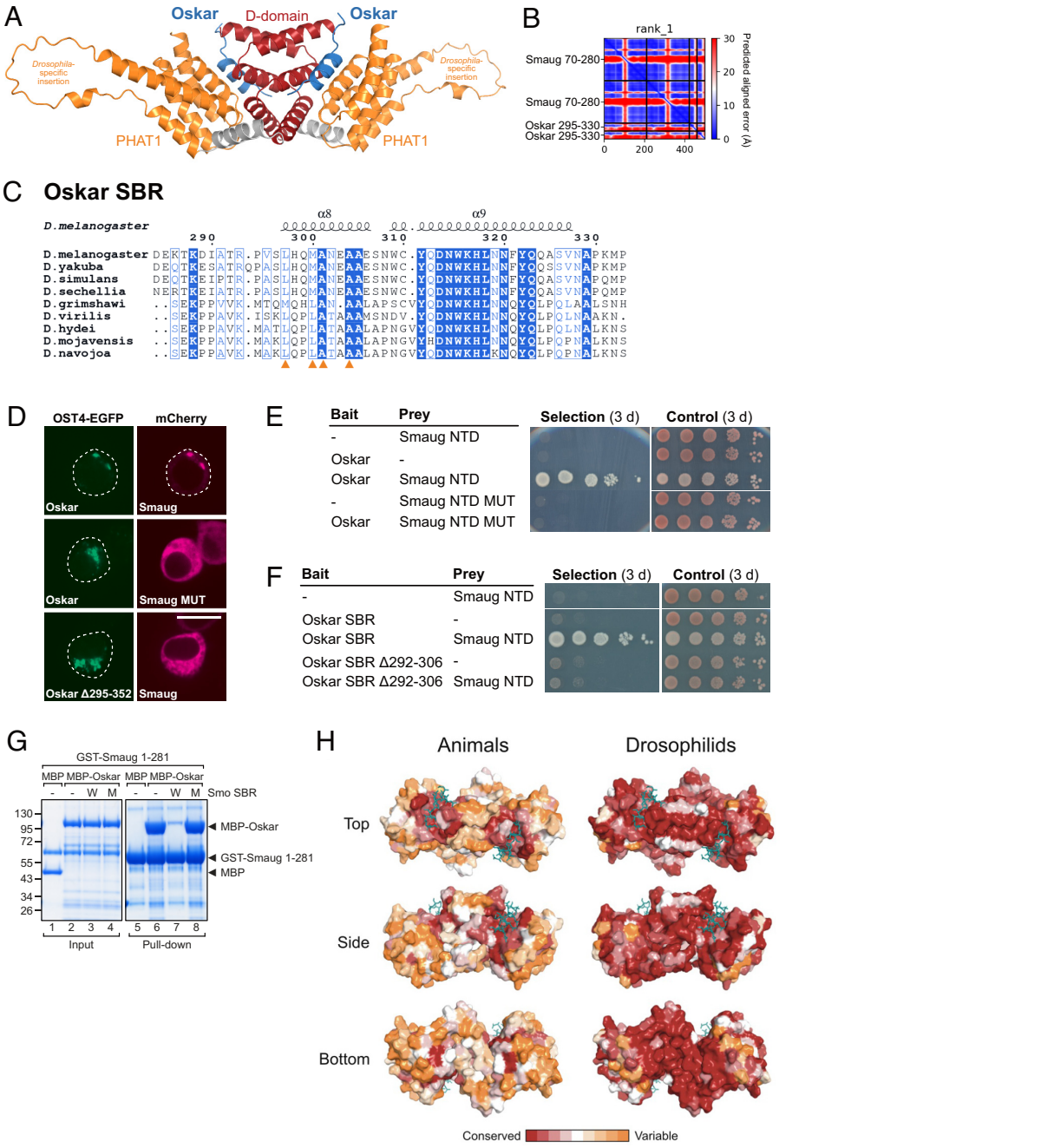

Fig. 5. Predicted structure of Smaug-NTD in complex with the Oskar SBR. (*A*) Structural model of the *Drosophila* Smaug-NTD in complex with the Oskar-SBR (blue) generated using AlphaFold2-multimer-version3 (58–60). The model contains the *Drosophila*-specific insertion (aa 156-196) of the Smaug-NTD. (*B*) Predicted aligned error plot generated from the prediction run, showing a low positional error of the N-terminal part of the Oskar-SBR relative to the Smaug-NTD. (*C*) Sequence alignment of Oskar covering the SBR. Orange triangles indicate Oskar residues that are critical for Smaug binding based on the predicted structural model. (*D*) OST4-EGFP and mCherry fusions to the proteins indicated were coexpressed in S2R+ cells, and their localization was analyzed by microscopy. The Smaug MUT (S250E, L253E) and the deletion of the SBR of Oskar (295-352) prevented the Smaug–Oskar interaction. (Scale bar is 10 μm.) (*E* and *F*) Yeast two-hybrid assays showing that the Smaug NTD MUT (S250E, L253E) or the deletion of aa 292-306 from the SBR (292-352) of Oskar prevented the Smaug–Oskar interaction. Selection medium lacked adenine and histidine. (*G*) GST pull-down assay using 1 nmol GST-Smaug 1-281 and 2 nmol His-MBP or His-MBP-Oskar. In addition, 45 nmol of a Smo 907-1003 synthetic peptide with wild-type (W) sequence or carrying the L978E/L984E/L985E point mutations (M) were present during the experiment as indicated above the gel image. Protein markers in kDa are indicated on the left. Input and pull-down samples originated from one experiment but were loaded onto two gels. (*H*) Surface representation of the Smaug NTD colored according to residue conservation (61) considering sequences of Smaug orthologs from various animals (*Left*) or Drosophilids only (*Right*).

Smaug phosphorylation was dependent on both Smoothened expression and HH signaling. Additional data suggested that upon HH signaling, Smoothened binds simultaneously to Smaug and the serine/threonine kinase Fused and thereby mediates the phosphorylation of Smaug by Fused (40). Using our ReLo assays, we confirmed a direct interaction between Smoothened and Fused and, consistent with previous Y2H data (73), we mapped Smoothened binding to the C-terminal regulatory domain of Fused (*SI Appendix*, Fig. S11*D*). Considering this chain of interactions and activities, we are wondering whether a Smaug phosphorylation event mediated by Smoothened might be relevant for the SCF-mediated ubiquitination and degradation of Smaug in

the early embryo. In this manner, Smoothened might contribute to the timing of the MZT in the early embryo, an exciting hypothesis that needs to be tested in the future.

Materials and Methods

Cloning of DNA Constructs. For the generation of the ReLo cloning vector pAc5.1-mEGFP (C-ter) (EB2), a unique FspAI restriction site was introduced 5′ of the mEGFP coding sequence of the pAc5.1-mEGFP vector (T6-MJ). The pAc5.1-OST4-EGFP vector (JK268) was generated by inserting the *S. cerevisiae* OST4 protein sequence amplified from pDHB1 (DualSystems Biotech) into the pAc5.1-EGFP plasmid (T5-MJ) using the KpnI restriction site. In the next step, the unique FspAI restriction site was introduced 3′ to the EGFP coding sequence. The FspAI sites were used to insert PCR-amplified inserts with blunt-end cloning. All other ReLo cloning vectors were described previously (45, 50, 74). The Y2H cloning vectors were described previously (27, 51). The pMJ-His *E. coli* expression vector was generated by introducing a unique ScaI blunt-end restriction site followed by a stop codon as close as possible downstream of the TEV protease recognition site of the pET-M11 vector. The pMJ-His-MBP vector was created by modification of the pET-M44 vector in a similar manner. The pMJ-GST vector was generated from the pGEX-6P-1 plasmid by introducing a unique SmaI blunt-end restriction site as close as possible downstream to the HRV 3C protease recognition sequence.

To generate the fusion construct for crystallization, the sequence of Smaug 73-278Δ156-196 was amplified from the pMJ-His-Smaug 70-281Δ156-196 plasmid (AG4) and ligated into the pMJ-His vector (T43-MJ) digested with ScaI. The sequence of Smo 970-1003 E975Q-$(GGS)_4$ was amplified from a synthetic DNA fragment codon-optimized for *E. coli* (gBlock from IDT) and ligated into the pMJ-His-Smaug 73-278Δ156-196 vector, which was opened by PCR amplification 5′ of the Smaug 73-278Δ156-196 sequence. Smo 970-1003 E975Q was deleted from the obtained plasmid by PCR amplification and Smo 970-1003 amplified from pAc 5.1-mEGFP-*Dm*-Smo 556-1035 (JK168) was inserted by blunt-end ligation. Detailed information on all plasmids used in this study is provided in *SI Appendix*, Table S2.

Protein Purification. Proteins were expressed using the autoinduction method (75). Briefly, Rosetta™ 2 competent cells (Novagen) were transformed with the protein expression vector and grown at 37 °C in LB medium supplemented with antibiotics. The following day, TB medium supplemented with antibiotics was inoculated with the overnight culture and grown at 22 °C or 23 °C for 27 h. For SeMet labeling of the *Hs*-SAMD4A 2-156 protein, the PASM-5052 expression medium (75) was used. Proteins were purified using affinity chromatography (Ni^{2+}-NTA or glutathione agarose), followed by ion exchange chromatography and size exclusion chromatography. For glutathione affinity chromatography, cells were lysed in lysis buffer (20 mM Tris-Cl, pH 7.5, 500 mM NaCl, 1 mM $MgCl_2$, 20% (w/v) glycerol, 2 mM β-mercaptoethanol) supplemented with 10 μg/mL DNase I (PanReac AppliChem) and ½ SIGMAFAST™ Protease inhibitor Cocktail Tablet (Sigma). The cleared lysate was incubated with 1 mL glutathione agarose (Pierce®) equilibrated in lysis buffer for 2 h at 4 °C. After washing with lysis buffer, proteins were eluted with a buffer containing 100 mM Tris-Cl pH 8, 500 mM NaCl, 20 mM reduced glutathione, and 20% (w/v) glycerol. For Ni^{2+}-NTA affinity chromatography, a similar procedure was followed with the following modifications: The lysis buffer contained 20 mM Tris-Cl, pH 7.5, 300 mM NaCl, 20 mM imidazole pH 7, 1 mM $MgCl_2$, 10% (w/v) glycerol, and 2 mM β-mercaptoethanol; the elution buffer contained 20 mM Tris-Cl, pH 7.5, 150 mM NaCl, 250 mM imidazole, pH 7, and 10% (w/v) glycerol, and the cleared lysate was incubated with 1 mL HisPur™ Ni-NTA Resin (ThermoFisher Scientific) for 30 to 60 min at 4 °C. For tag removal, 1 mg His-TEV protease was used per 10 mg protein. The purification step using the HiPrep Q XL 16/10 ion exchange column was performed in a buffer containing 20 mM Tris-Cl, pH 9, 50 mM NaCl, and 10% (w/v) glycerol with a gradient elution up to 1M NaCl. Proteins were eluted from the final size exclusion chromatography column in a buffer containing 20 mM Tris-Cl, pH 7.5, and 150 mM NaCl. In the case of the GST, His-MBP, and His-MBP-Oskar 292-325 proteins, the elution buffer contained 10% (w/v) glycerol in addition.

Protein–Protein Interaction Assays. ReLo assays were described previously (45). In brief, *Drosophila* S2R+ cells were seeded onto a 4-well polymer μ-Slide (Ibidi) and cotransfected with the desired combination of plasmids using jetOPTIMUS transfection reagent (Polyplus). After incubation for 24–48 h at 25 °C, images of the cells were taken with a CFI Plan Apochromat Lambda D 100 × oil objective and a Nikon Ti-E spinning disc confocal fluorescence microscope and processed using Fiji software (76). The individual cell(s) shown in the figures are representative of the whole cotransfected cell population. Cotransfection experiments were performed two to six times (also counting experiments with swapped tags). Some ReLo experiments were done only once, and with the exception of one (*SI Appendix*, Fig. S11*C*), they were confirmed by or consistent with data generated using other assays (Figs. 3*E* and 5*D* and *SI Appendix*, Fig. S7A).

Y2H assays were performed as in ref. 51. Briefly, *S. cerevisiae* NMY51 cells were cotransformed with the desired combination of plasmids, plated on a control Synthetic Defined Complete (SDC) agar plate (lacking Leu, Trp) and incubated at 30 °C for 48 to 72 h. For the spot assay, the cells from several colonies were resuspended in distilled water to an OD600 of 0.5. Four consecutive 10-fold serial dilutions were prepared and spotted on a selection plate (SDC lacking Leu, Trp, His, Ade) and a control plate (SDC lacking Leu, Trp). Plates were incubated at 30 °C for the number of days as indicated in the figure legends.

GST pull-down assays were performed essentially as described (50). In short, the proteins as indicated in the figure legends were incubated for 30 min at 25 °C in incubation buffer [20 mM Tris-Cl, pH 7.5, 150 mM NaCl, 10% (w/v) glycerol, 5 mM DTT, and 0.1% Tween-20]. Subsequently, 40 μL of a 1:2 slurry of glutathione agarose (Pierce™, ThermoFisher Scientific) in incubation buffer was added, and the mixture was incubated for additional 90 to 120 min with interval mixing. The resin was then washed five times with 1 mL incubation buffer. Proteins were eluted with SDS sample buffer, separated by SDS PAGE, and stained with PageBlue Protein Staining Solution. MBP pull-down assays were performed similar to GST pull-down assays using amylose resin (New England Biolabs).

ITC was performed at 15 °C using a MicroCal PEAQ instrument (Malvern Panalytical Ltd) and a buffer containing 20 mM Tris-Cl, pH 7.5, and 150 mM NaCl. The syringe contained 200 μM of Smaug 70-281 protein, which was titrated in 19 injections into the cell containing 20 μM of a Smoothened 970-1003 synthetic peptide (Peptide Specialty Laboratories GmbH, Germany). The first injection consisted of 0.4 μL, the consecutive injections had 2 μL. Reference power was set to 10 μW; the stir speed was 750 rpm. In the control experiment, the buffer was titrated into the cell with the peptide. The results were fitted and analyzed with the MicroCal PEAQ-ITC Analysis Software.

The Smoothened peptide sequences used for the GST pull-down competition and/or the ITC experiments were VPSYGEDELQQAMRLLNAASRQRTEAANEDFGGT (wild-type) and VPSYGEDEEQQAMREENAASRQRTEAANEDFGGT (L978E/L984E/L985E mutant).

Crystallization and Structure Determination. The crystallization of human His-SAMD4A 2-156 was performed using the hanging drop vapor diffusion method. First, 2 μL native (23 mg/mL) or SeMet-labeled protein (37.5 mg/mL) in crystallization buffer (20 mM Tris-Cl, pH 7.5, and 150 mM NaCl, supplemented with 5 mM DTT) were mixed with 2 μL precipitant (0.1 M sodium citrate, pH 5.6, and 8% jeffamine M-600, pH 7) and incubated at 18 °C. Then, crystals appeared after 1 d and were cryogenically protected by supplementing them with 35% or 40% (v/v) glycerol prior to flash-freezing in liquid nitrogen. Diffraction data for native and SeMet crystals were collected at the P14 beamline using 0.9686 Å and at the P13 beamline using 0.9800 Å, respectively, operated by EMBL Hamburg at the PETRA III storage ring (DESY, Hamburg, Germany). The diffraction data were processed anisotropically using STARANISO (Global Phasing Limited). The phases were determined with multiwavelength anomalous dispersion using the reflections from the peak of SeMet derivatives and the native crystal using the AutoSol program of the PHENIX suite (77).

The Smoothened 970-1003-$(GGS)_4$-Smaug 73-278Δ156-196 fusion protein (His-tag removed) at 11.6 mg/mL concentration (supplemented with 5 mM DTT) was crystallized by mixing with an equal volume of precipitant [0.1 M HEPES, pH 7.5, 5% (w/v) PEG3000, and 20% (w/v) PEG400] using the sitting-drop vapor diffusion method at 18 °C. Rod/needle-shaped single crystals appeared after 7 d. The crystals were cryogenically protected by supplementing them with 10% glycerol prior to flash-freezing in liquid nitrogen. The diffraction data were collected at the ID-30B beamline at the ESRF (Grenoble, France) and processed anisotropically using STARANISO (Global Phasing Limited). The structure was solved by molecular replacement using the structure of the SAMD4A-NTD dimer as a search template. Structures were refined using phenix.refine and Coot (78, 79) and figures were generated using PyMol. All data collection and refinement statistics are provided in *SI Appendix*, Table S1.

For the AlphaFold2 predictions, the ColabFold v1.5.2 web interface (60) was used with standard settings except for the model_type, which was switched from "auto" to "alphaFold2_multimer_v3".

Data, Materials, and Software Availability. The structures reported here have been deposited to the Protein Data Bank (PDB) and are available under accession numbers 8OIK (SAMD4A-NTD) (80) and 8OIJ (Smaug-NTD–Smoothened peptide complex) (81).

ACKNOWLEDGMENTS. We thank Timo Färber, Anastasija Gricenko, Felia Haffelder, David Hauser, Harpreet Kaur Salgania, Maik Schauerte, Alina Schneider, Jonas Weidenhausen, Julan Weng, and Janka Zsok for technical support. We thank Elisa Izaurralde for plasmids. We thank Elmar Wahle, Craig Smibert, and Julien Béthune for constructive feedback on the manuscript. We thank the Nikon Imaging Center at the University of Heidelberg for access to microscopes and the BZH Protein Crystallization Platform. We gratefully acknowledge the P13 and P14 beamlines operated by EMBL Hamburg at the PETRA III storage ring (DESY, Hamburg, Germany) and the ID-30B beamline at the ESRF (Grenoble, France), and Isabel Bento (DESY) and Nicolas Coquelle (ESRF) for the assistance in using the beamlines. We gratefully acknowledge the data storage service SDS@hd supported by the Ministry of Science, Research and the Arts Baden-Württemberg (MWK) and the German Research Foundation (DFG) through the grants INST 35/1314-1 FUGG and INST 35/1503-1 FUGG. This work was funded by the Emmy-Noether Program of the German Research Foundation (DFG; JE-827/1-1).

1. P. Lasko, Posttranscriptional regulation in *Drosophila* oocytes and early embryos. *Wiley Interdiscip Rev. RNA* **2**, 408–416 (2011).
2. D. Lazzaretti, F. Bono, mRNA localization in metazoans: A structural perspective. *RNA Biol.* **14**, 1473–1484 (2017).
3. D. R. Schoenberg, L. E. Maquat, Regulation of cytoplasmic mRNA decay. *Nat. Rev. Genet.* **13**, 246–259 (2012).
4. M. R. Fabian, N. Sonenberg, The mechanics of miRNA-mediated gene silencing: A look under the hood of miRISC. *Nat. Struct. Mol. Biol.* **19**, 586–593 (2012).
5. Y. Lee, J. Choe, O. H. Park, Y. K. Kim, Molecular mechanisms driving mRNA degradation by m6A modification. *Trends Genet.* **36**, 177–188 (2020).
6. C. D. Thanos, K. E. Goodwill, J. U. Bowie, Oligomeric structure of the human EphB2 receptor SAM domain. *Science* **1979**, 833–836 (1999).
7. J. Schultz, C. P. Ponting, K. Hofmann, P. Bork, SAM as a protein interaction domain involved in developmental regulation. *Protein Sci.* **6**, 249–253 (1997).
8. F. Qiao, J. U. Bowie, The many faces of SAM. *Sci. STKE.* **2005**, re7 (2005).
9. G. Amadei *et al.*, A Smaug2-based translational repression complex determines the balance between precursor maintenance versus differentiation during mammalian neurogenesis. *J. Neurosci.* **35**, 15666–15681 (2015).
10. T. Aviv *et al.*, The RNA-binding SAM domain of Smaug defines a new family of post-transcriptional regulators. *Nat. Struct. Biol.* **10**, 614–621 (2003).
11. M. V. Baez, G. L. Boccaccio, Mammalian Smaug is a translational repressor that forms cytoplasmic foci similar to stress granules. *J. Biol. Chem.* **280**, 43131–40 (2005).
12. J. B. Green, C. D. Gardner, R. P. Wharton, A. K. Aggarwal, RNA recognition via the SAM domain of Smaug. *Mol. Cell* **11**, 1537–1548 (2003).
13. N. Niu *et al.*, RNA-binding protein SAMD4 regulates skeleton development through translational inhibition of Mig6 expression. *Cell Discov.* **3**, 16050 (2017).
14. P. E. Johnson, L. W. Donaldson, RNA recognition by the Vts1p SAM domain. *Nat. Struct. Mol. Biol.* **13**, 177–178 (2006).
15. T. Aviv, Z. Lin, G. Ben-Ari, C. A. Smibert, F. Sicheri, Sequence-specific recognition of RNA hairpins by the SAM domain of Vts1p. *Nat. Struct. Mol. Biol.* **13**, 168–176 (2006).
16. F. C. Oberstrass *et al.*, Shape-specific recognition in the structure of the Vts1p SAM domain with RNA. *Nat. Struct. Mol. Biol.* **13**, 160–167 (2006).
17. X. Tang *et al.*, Suprafacial orientation of the SCF Cdc4 dimer accommodates multiple geometries for substrate ubiquitination. *Cell* **129**, 1165–1176 (2007).
18. Z. Chen *et al.*, Mutation of mouse Samd4 causes leanness, myopathy, uncoupled mitochondrial respiration, and dysregulated mTORC1 signaling. *Proc. Natl. Acad. Sci. U.S.A.* **111**, 7367–7372 (2014).
19. A. Dahanukar, R. P. Wharton, The *nanos* gradient in *Drosophila* embryos is generated by translational regulation. *Genes Dev.* **10**, 2610–2620 (1996).
20. A. Dahanukar, J. A. Walker, R. P. Wharton, Smaug, a novel RNA-binding protein that operates a translational switch in *Drosophila*. *Mol. Cell* **4**, 209–218 (1999).
21. C. A. Smibert, J. E. Wilson, K. Kerr, P. M. Macdonald, smaug protein represses translation of unlocalized *nanos* mRNA in the *Drosophila* embryo. *Genes Dev.* **10**, 2600–2609 (1996).
22. M. Götze *et al.*, Translational repression of the *Drosophila nanos* mRNA involves the RNA helicase Belle and RNA coating by Me31B and Trailer hitch. *RNA* **23**, 1552–1568 (2017).
23. M. Jeske, B. Moritz, A. Anders, E. Wahle, Smaug assembles an ATP-dependent stable complex repressing *nanos* mRNA translation at multiple levels. *EMBO J.* **30**, 1–9 (2011).
24. M. R. Nelson, A. M. Leidal, C. A. Smibert, *Drosophila* cup is an eIF4E-binding protein that functions in Smaug-mediated translational repression. *EMBO J.* **23**, 150–159 (2004).
25. J. L. Semotok *et al.*, Smaug recruits the CCR4/POP2/NOT deadenylase complex to trigger maternal transcript localization in the early *Drosophila* embryo. *Curr. Biol.* **15**, 284–294 (2005).
26. S. Zaessinger, I. Busseau, M. Simonelig, Oskar allows *nanos* mRNA translation in *Drosophila* embryos by preventing its deadnylation by Smaug/CCR4. *Development* **133**, 4573–4583 (2006).
27. F. Pekovic *et al.*, RNA binding proteins Smaug and Cup induce CCR4-NOT-dependent deadenylation of the *nanos* mRNA in a reconstituted system. *Nucleic Acids Res.* **51**, 3950–3970 (2023).
28. B. D. Pinder, C. A. Smibert, MicroRNA-independent recruitment of Argonaute 1 to *nanos* mRNA through the Smaug RNA-binding protein. *EMBO Rep.* **14**, 80–86 (2013).
29. C. Wang, R. Lehmann, Nanos is the localized posterior determinant in *Drosophila*. *Cell* **66**, 637–647 (1991).
30. C. Wang, L. K. Dickinson, R. Lehmann, Genetics of *nanos* localization in *Drosophila*. *Dev. Dyn.* **199**, 103–115 (1994).
31. E. R. Gavis, R. Lehmann, Localization of *nanos* RNA controls embryonic polarity. *Cell* **71**, 301–313 (1992).
32. E. R. Gavis, R. Lehmann, Translational regulation of *nanos* by RNA localization. *Nature* **369**, 315–318 (1994).
33. B. Benoit *et al.*, An essential role for the RNA-binding protein Smaug during the *Drosophila* maternal-to-zygotic transition. *Development* **136**, 923–932 (2009).
34. L. Chen *et al.*, Global regulation of mRNA translation and stability in the early *Drosophila* embryo by the Smaug RNA-binding protein. *Genome Biol.* **15**, 19–22 (2014).
35. N. U. Siddiqui *et al.*, Genome-wide analysis of the maternal-to-zygotic transition in *Drosophila* primordial germ cells. *Genome Biol.* **13**, R11 (2012).
36. W. Tadros *et al.*, SMAUG is a major regulator of maternal mRNA destabilization in *Drosophila* and its translation is activated by the PAN GU kinase. *Dev. Cell* **12**, 143–155 (2007).
37. W. X. Cao *et al.*, Precise temporal regulation of post-transcriptional repressors is required for an orderly *Drosophila* maternal-to-zygotic transition. *Cell Rep.* **31**, 107783 (2020).
38. C. A. Smibert, Y. S. Lie, W. Shillinglaw, W. J. Henzel, P. M. Macdonald, Smaug, a novel and conserved protein, contributes to repression of *nanos* mRNA translation in vitro. *RNA* **5**, 1535–1547 (1999).
39. W. X. Cao, A. Karaiskakis, S. Lin, S. Angers, H. D. Lipshitz, The F-box protein Bard (CG14317) targets the Smaug RNA-binding protein for destruction during the *Drosophila* maternal-to-zygotic transition. *Genetics* **220**, iyab177 (2022).
40. L. Bruzzone *et al.*, Regulation of the RNA-binding protein Smaug by the GPCR Smoothened via the kinase Fused. *EMBO Rep.* **21**, 1–16 (2020).
41. P. W. Ingham, A. P. McMahon, Hedgehog signaling in animal development: Paradigms and principles. *Genes Dev.* **15**, 3059–3087 (2001).
42. L. Holm, P. Rosenström, Dali server: Conservation mapping in 3D. *Nucleic Acids Res.* **38**, 545–549 (2010).
43. E. Krissinel, K. Henrick, Inference of macromolecular assemblies from crystalline state. *J. Mol. Biol.* **372**, 774–797 (2007).
44. S. W. Englander, L. Mayne, The nature of protein folding pathways. *Proc. Natl. Acad. Sci. U.S.A.* **111**, 15873–15880 (2014).
45. H. K. Salgania, J. Metz, M. Jeske, ReLo is a simple and quick colocalization assay to identify and characterize direct protein-protein interactions. bioRxiv [Preprint] (2022). https://www.biorxiv.org/content/10.1101/2022.03.04.482790v2 (Accessed 17 July 2023).
46. B. Barckmann *et al.*, Aubergine iCLIP reveals piRNA-dependent decay of mRNAs involved in germ cell development in the early embryo. *Cell Rep.* **12**, 1205–1216 (2015).
47. C. Rouget *et al.*, Maternal mRNA deadenylation and decay by the piRNA pathway in the early *Drosophila* embryo. *Nature* **467**, 1128–1132 (2010).
48. F. H. Markussen, A. M. Michon, W. Breitwieser, A. Ephrussi, Translational control of *oskar* generates short OSK, the isoform that induces pole plasm assembly. *Development* **121**, 3723–3732 (1995).
49. N. Vanzo, A. Oprins, D. Xanthakis, A. Ephrussi, C. Rabouille, Stimulation of endocytosis and actin dynamics by oskar polarizes the *Drosophila* oocyte. *Dev. Cell* **12**, 543–555 (2007).
50. M. Jeske, C. W. Müller, A. Ephrussi, The LOTUS domain is a conserved DEAD-box RNA helicase regulator essential for the recruitment of Vasa to the germ plasm and nuage. *Genes Dev.* **31**, 939–952 (2017).
51. M. Jeske *et al.*, The crystal structure of the *Drosophila* germline inducer Oskar identifies two domains with distinct Vasa Helicase- and RNA-binding activities. *Cell Rep.* **12**, 587–598 (2015).
52. J. Anne, Targeting and anchoring Tudor in the pole plasm of the *Drosophila* oocyte. *PLoS One* **5**, e14362 (2010).
53. C. Ottone, S. Gigliotti, A. Giangrande, F. Graziani, A. V. di Pianella, The translational repressor cup is required for germ cell development in *Drosophila*. *J. Cell Sci.* **125**, 3114–3123 (2012).
54. R. Suyama, A. Jenny, S. Curado, W. Pellis-van Berkel, A. Ephrussi, The actin-binding protein Lasp promotes Oskar accumulation at the posterior pole of the *Drosophila* embryo. *Development* **136**, 95–105 (2009).
55. W. Breitwieser, F. H. Markussen, H. Horstmann, A. Ephrussi, Oskar protein interaction with vasa represents an essential step in polar granule assembly. *Genes Dev.* **10**, 2179–2188 (1996).
56. D. Ding *et al.*, LOTUS domain is a novel class of G-rich and G-quadruplex RNA binding domain. *Nucleic Acids Res.* **48**, 9262–9272 (2020).
57. N. Yang *et al.*, Structure of *Drosophila* Oskar reveals a novel RNA binding protein. *Proc. Natl. Acad. Sci. U.S.A.* **112**, 11541–11546 (2015).
58. R. Evans *et al.*, Protein complex prediction with AlphaFold-Multimer. bioRxiv [Preprint] (2021). https://www.biorxiv.org/content/10.1101/2021.10.04.463034v2 (Accessed 17 July 2023).
59. J. Jumper *et al.*, Highly accurate protein structure prediction with AlphaFold. *Nature* **596**, 583–589 (2021).
60. M. Mirdita *et al.*, ColabFold: Making protein folding accessible to all. *Nat. Methods* **19**, 679–682 (2022).
61. H. Ashkenazy *et al.*, ConSurf 2016: An improved methodology to estimate and visualize evolutionary conservation in macromolecules. *Nucleic Acids Res.* **44**, W344–W350 (2016).
62. K. A. Dean, A. K. Aggarwal, R. P. Wharton, Translational repressors in *Drosophila*. *Trends Genet.* **18**, 572–576 (2002).
63. L. S. Gramates *et al.*, FlyBase: A guided tour of highlighted features. *Genetics* **220**, iyac035 (2022).
64. N. Casas-Vila *et al.*, The developmental proteome of *Drosophila melanogaster*. *Genome Res.* **27**, 1273–1285 (2017).
65. M. van den Heuvel, P. W. Ingham, Required for hedgehog signalling. *Lett. Nat.* **382**, 413–417 (1996).
66. E. Morais-de-Sá, A. Vega-Rioja, V. Trovisco, D. StJohnston, Oskar is targeted for degradation by the sequential action of Par-1, GSK-3, and the SCF-Slimb ubiquitin ligase. *Dev. Cell* **26**, 303–314 (2013).
67. B. Mason, H. Laman, The FBXL family of F-box proteins: Variations on a theme: The FBXL family of F-box proteins. *Open Biol.* **10**, 200319 (2020).
68. D. Frescas, M. Pagano, Deregulated proteolysis by the F-box proteins SKP2 and β-TrCP: Tipping the scales of cancer. *Nat. Rev. Cancer* **8**, 438–449 (2008).

69. J. Jia *et al.*, Phosphorylation by double-time/CKIε and CKIα targets cubitus interruptus for slimb/β-TRCP-mediated proteolytic processing. *Dev. Cell* **9**, 819–830 (2005).
70. J. Fehilly *et al.*, Condensate formation of the human RNA-binding protein SMAUG1 is controlled by its intrinsically disordered regions and interactions with 14-3-3 proteins. bioRxiv [Preprint] (2023). https://doi.org/10.1101/2023.02.09.527857 (Accessed 17 July 2023).
71. V. Obsilova, T. Obsil, Structural insights into the functional roles of 14-3-3 proteins. *Front. Mol. Biosci.* **9**, 1044 (2022).
72. B. Zhai, J. Villén, S. A. Beausoleil, J. Mintseris, S. P. Gygi, Phosphoproteome Analysis of *Drosophila melanogaster* Embryos. *J. Proteome Res.* **7**, 1675–1682 (2008).
73. S. Malpel *et al.*, The last 59 amino acids of Smoothened cytoplasmic tail directly bind the protein kinase Fused and negatively regulate the Hedgehog pathway. *Dev. Biol.* **303**, 121–133 (2007).
74. I. Behm-Ansmant *et al.*, mRNA degradation by miRNAs and GW182 requires both CCR4:NOT deadenylase and DCP1:DCP2 decapping complexes. *Genes Dev.* **20**, 1885–1898 (2006).
75. F. W. Studier, Protein production by auto-induction in high density shaking cultures. *Protein Expr. Purif.* **41**, 207–234 (2005).
76. J. Schindelin *et al*. Fiji: An open-source platform for biological-image analysis. *Nat. Methods* **9**, 676–682 (2012).
77. P. D. Adams *et al.*, PHENIX: A comprehensive Python-based system for macromolecular structure solution. *Acta Crystallogr. D Biol. Crystallogr.* **66**, 213–221 (2010).
78. P. V. Afonine *et al.*, Towards automated crystallographic structure refinement with phenix.refine. *Acta Crystallogr. D Biol. Crystallogr.* **68**, 352–367 (2012).
79. P. Emsley, K. Cowtan, Coot: Model-building tools for molecular graphics. *Acta Crystallogr. D Biol. Crystallogr.* **60**, 2126–2132 (2004).
80. J. Kubikova, M. Jeske, D-PHAT domain (NTD) of human SAMD4A. Protein Data Bank. https://doi.org/10.2210/pdb8oik/pdb. Accessed 17 July 2023b.
81. G. Ubartaite, J. Kubikova, M. Jeske, *Drosophila* Smaug-Smoothened complex. Protein Data Bank. https://doi.org/10.2210/pdb8oij/pdb. Accessed 17 July 2023a.